Natural Aging in Mg-Zn(-Cu) Alloys

J. BUHA and T. OHKUBO

Natural aging in Mg-Zn-Cu alloys results in a significant hardening due to the formation of a high number density of shearable precipitates. For alloys containing Zn and Cu in the compositional ranges of both cast and wrought alloys (Zn = 2 to 2.4 at. pct, and Cu = 0.15 to 1.2 at. pct), hardening produced by natural aging (T4) for 4 to 8 weeks (91 to 104 VHN) almost equals that produced by artificial aging (93 to 109 VHN). The density of the precipitates in the T4 condition of Mg-Zn-Cu alloys was found to be of the order of precipitate density in a typical aged aluminum alloy (10^{24} precipitates/m^3). An addition of even a trace amount of Cu to Mg-Zn alloy enhances the nucleation of the precipitates and accelerates the kinetics of precipitation, in particular during natural aging. This is believed to be a result of the enhanced favorable interaction between Cu, Zn, and vacancies. The strengthening is produced mainly by the formation of a very high density of the coherent disc-shaped Guinier–Preston 1 (GP1) zones and the prismatic precipitates perpendicular to the magnesium basal plane.

DOI: 10.1007/s11661-008-9545-y

I. INTRODUCTION

MAGNESIUM alloys containing Zn as the major alloying element are known to have a marked response to precipitation hardening. Due to problems with hot shortness, brittleness, and coarse and uneven grain size in binary Mg-Zn alloys, commercially interesting alloys are always grain refined by the addition of Zr (ZK series alloys). Alloying with rare earth elements such as Ce, Nd, La, Pr, and Gd, often combined in the form of misch metal, improves both casting characteristics and mechanical properties at elevated temperatures (ZE and EZ series);[1] however, this also increases the alloy cost. Alloying with Cu is cost effective, and as Unsworth and King[2,3] reported, Mg-Zn-Cu alloys (ZC series), apart from having good casting characteristics, also have a significantly increased age-hardening response compared to binary Mg-Zn alloy. Addition of Cu also increases the eutectic temperature and permits the use of higher solution treatment temperatures.[2,3] The precipitation sequence in the Cu-containing Mg-Zn alloys above 150 °C[4] has been reported to be the same as the most probable aging sequence for a binary Mg-Zn alloy:[5–12]

$$\begin{aligned}&\text{SSSS} \rightarrow \text{solute clusters} \rightarrow \text{GP zones/pre-}\beta' \\ &\rightarrow \beta'_1 \text{ rods, blocks} \perp \{0001\}_{Mg};\ (\text{possibly } Mg_4Zn_7) \\ &\rightarrow \beta'_2 \text{ discs}\|\{0001\}_{Mg};\ \text{laths} \perp \{0001\}_{Mg};\ (MgZn_2) \\ &\quad\rightarrow \beta \text{ equilibrium phase (MgZn or } Mg_2Zn_3)\end{aligned}$$

The structure, composition, and thermal stability of some of these phases have not yet been fully clarified and agreed upon; however, a number of reports agree that the maximum hardening due to the precipitation in Mg-Zn alloys is associated with the formation of the rod-shaped transition β'_1 phase. Earlier reports stated that this phase formed possibly *via* another transition phase denoted pre-β' (still uncharacterized) and had a composition and a crystal structure indistinguishable from that of the Laves $MgZn_2$ phase.[5,9] A more recent study, however, shows that the crystal structure of the β'_1 is similar to that of Mg_4Zn_7 phase.[11] A smaller fraction of this phase may also exhibit a blocky morphology.[11] In addition to the β'_1 rods, a lath-shaped form of the β'_2 phase ($MgZn_2$) may also form in the artificially aged condition.[11] On overaging, the rods and laths are gradually replaced by a coarse plate-shaped form of the β'_2 phase.[5,9] The equilibrium β phase, MgZn[5] or Mg_2Zn_3,[9] may form upon high overaging; however, its crystal structure is still unknown. In the Cu-containing alloys, the precipitates were found to be finer, and more uniformly and far more densely distributed, than in the binary alloy.[4] This was one of the main reasons for the superior mechanical properties of the ZC series alloys.[2,3] The precipitation in Mg-Zn–based alloys at reduced temperatures ($\sim < 110$ °C) has not been commonly studied. Three types of Guinier–Preston (GP) zones were reported to form in these alloys, mainly at lower temperatures. The X-ray diffraction studies on Mg-3.6 wt pct Zn alloy by Takahashi *et al.*[13] showed that at temperatures below 60 °C, "GP1" zones formed directly from the solid solution as plates parallel to $\{11\bar{2}0\}_{Mg}$ planes, while below 80 °C, "GP2" zones formed in the form of oblate spheroids on $\{0001\}_{Mg}$ planes. The disclike "GP" zones were reported to form parallel to $\{0001\}_{Mg}$ planes.[14] The precipitation of GP zones was also confirmed by the effect that low-temperature preaging had on hardness and microstructure evolution

J. BUHA, formerly JSPS Fellow, National Institute for Materials Science, is Research Fellow, School of Materials Science and Engineering, University of New South Wales, Sydney NSW 2052, Australia. Contact e-mail: jokabuha@yahoo.com T. OHKUBO, Group Leader, is with the National Institute for Materials Science, Tsukuba 305-0047, Japan.

Manuscript submitted February 13, 2007.
Article published online May 22, 2008

during subsequent artificial aging.[7,8,15] A more recent study showed that the precipitation in Mg-Zn alloy commences by clustering of Zn atoms, while during aging at intermediate temperatures (up to about 100 °C), four to six different types of precipitates were simultaneously present in the microstructure leading to hardening of a significant magnitude.[16]

Age hardening at ambient temperature after quenching from the solution heat treatment temperature is common to age-hardenable aluminum alloys; however, this was not observed in age-hardenable magnesium alloys in the past.[5,7] This led to an assumption that magnesium alloys do not undergo natural aging and that the interactions between the solute elements and vacancies in these alloys are weak. On the other hand, for some aluminum alloys (*e.g.*, Al-Cu-Li-Ag-Mg-Zr), the mechanical properties achieved by natural aging can reach those of the artificially aged material;[17] for some Al-Zn-Mg (7000 series) and Al-Cu-Mg (2000 series) based alloys, natural aging prior to artificial aging may, in some cases, be beneficial to the mechanical properties of the artificially aged material. The recent study, however, shows that magnesium alloys also undergo appreciable hardening at ambient temperature and that, for Mg-Zn based alloys in particular, hardness in the T4 condition eventually nearly equals that in the T6.[16] The kinetics of natural aging depends strongly on alloy composition, and some alloys harden to near T6 hardness level within a few weeks, while others (*e.g.*, binary Mg-Zn alloy and ZK60) require several months.[16] The alloys containing Cu are among those that undergo rapid hardening at ambient temperature. This article describes in detail the microstructures produced by natural aging in a number of alloys having different contents of Cu and discusses in detail the effect of the Cu content on the nucleation of precipitates and kinetics of natural aging. The development of microstructure during both natural and artificial aging of Mg-Zn-Cu alloys was investigated by hardness measurements, conventional transmission electron microscopy (TEM), high-resolution transmission electron microscopy (HR TEM), and three-dimensional atom probe (3DAP), and compared to that of the binary Mg-Zn alloy. In particular, 3DAP was used to determine the composition of some of the major strengthening phases forming during aging.

Table I. Chemical Composition of the Mg-Zn(-Cu) Alloys in Atomic Percent and in Weight Percent (Given in Parentheses)

Element, At. Pct (Wt Pct)	Mg	Zn	Cu	Mn
Binary	balance	2.8 (7)	(< 0.01)	(< 0.01)
A		2.4 (6)	1.2 (3)	0.04 (0.1)
B		2.4 (6)	0.3 (0.8)	0.04 (0.1)
C		2 (4.6)	0.15 (0.4)	(< 0.01)
D		1 (2.6)	0.5 (1.2)	(< 0.01)

II. EXPERIMENTAL PROCEDURES

Alloys were prepared from Mg of 99.8 pct purity, Mg-Zn, Mg-Mn, and Mg-Cu prealloys by induction melting under the protective argon atmosphere and cast into a permanent mold as rods of 15 mm in diameter and about 100 mm in length. The alloy compositions determined by the X-ray florescence and by the inductively coupled plasma–optical emission spectrometry methods on multiple alloy samples in the homogenized condition are listed in Table I. All alloys contained trace impurities of Fe (0.05 to 0.08 wt pct), Al (< 0.01 to 0.07 wt pct), and Si (< 0.01 to 0.08 wt pct). Note that the compositions (in at. pct) of alloys Mg-2.4Zn-1.2Cu-0.04Mn (A) and Mg-2.4Zn-0.3Cu-0.04Mn (B) are, with the exception of a considerably lower Mn content, very similar to the compositions of the commercial alloys ZC63 (cast alloy) and ZCM711 (wrought alloy), respectively.[2] The details of the heat treatments for each alloy are given in Table II. During the homogenization and solution heat treatment, alloy specimens were sealed in a Pyrex tube partially filled with argon to prevent oxidation. The alloys were aged in an oil bath at 160 °C (T6) and in air at room temperature (T4). Microhardness measurements were made on aged specimens and the results reported here are averaged from at least 12 measurements. The consistency of these measurements was confirmed between loads of 50 and 300 g. The average grain size of alloy specimens in the as-solution-treated condition was determined following the planimetric method described in the ASTM standard E 112-96 (2004) and using five randomly selected fields for each alloy specimen. Optical microscopy images were taken from alloys in the as-solution-treated condition after etching the polished specimens using acetic picral[18] in order to reveal grain boundaries. Specimens for the TEM observations were prepared from the aged material by electropolishing in a solution of 22.32 g $Mg(ClO_4)_2$ and 10.6 g LiCl in 1000 mL of methanol and 200 mL of 2-butoxi-ethanol

Table II. Heat Treatment Procedures

Alloy	Homogenization		Solution Treatment		Aging
Binary	315 °C–48 h	cold water quench	315 °C–5 h	cold water quench	at 160 °C and at room temperature
	335 °C–96 h		340 °C–5 h		
A	440 °C–48 h		440 °C–5 h		
B	390 °C–48 h		390 °C–5 h		
C	435 °C–48 h		435 °C–5 h		
D	440 °C–48 h		440 °C–5 h		

at about –45 °C and 90 V. Conventional TEM observations and the energy dispersive spectroscopy (EDS) analysis were performed using a PHILIPS* CM200 microscope operated at 200 kV. The precipitate length was measured using Image Tool 3.00 software (The University of Texas Health Science Center, San Antonio, Texas)[19] from at least four TEM images taken from specimens of similar thickness and with a grain orientation close to either $[2\bar{1}\bar{1}0]_{Mg}$ or $[0\bar{1}10]_{Mg}$ in order to minimize the number of precipitates cut by the foil surface. For the TEM specimen from the binary Mg-Zn alloy in the T6 condition, a slightly higher foil tilt was needed, and many precipitates were truncated by the foil surface; thus, the measurement reported for this alloy is likely to be an underestimate of the real length. The HRTEM observations were performed using an FEI Tecnai G2 F30 microscope (FEI Company, Hillsboro, Oregon) operated at 300 kV. The atomic distributions of alloys were analyzed using an energy compensated 3DAP equipped with a delay line detector,[20–22] at a specimen temperature of ~30 K in an ultrahigh vacuum of $\sim 10^{-8}$ Pa and with a voltage pulse fraction of 15 pct. Sharp needle-shaped specimens were prepared by cutting square rods (blanks) from the aged bulk specimens, which were then electropolished following the standard two-stage electropolishing method. Visualization and the analysis of the 3DAP data were performed using PoSAP 1.7 software (Oxford nanoScience Ltd., Kiln Farm, UK).[22]

*PHILIPS is a trademark of Philips Electronic Instruments Corp., Mahwah, NJ.

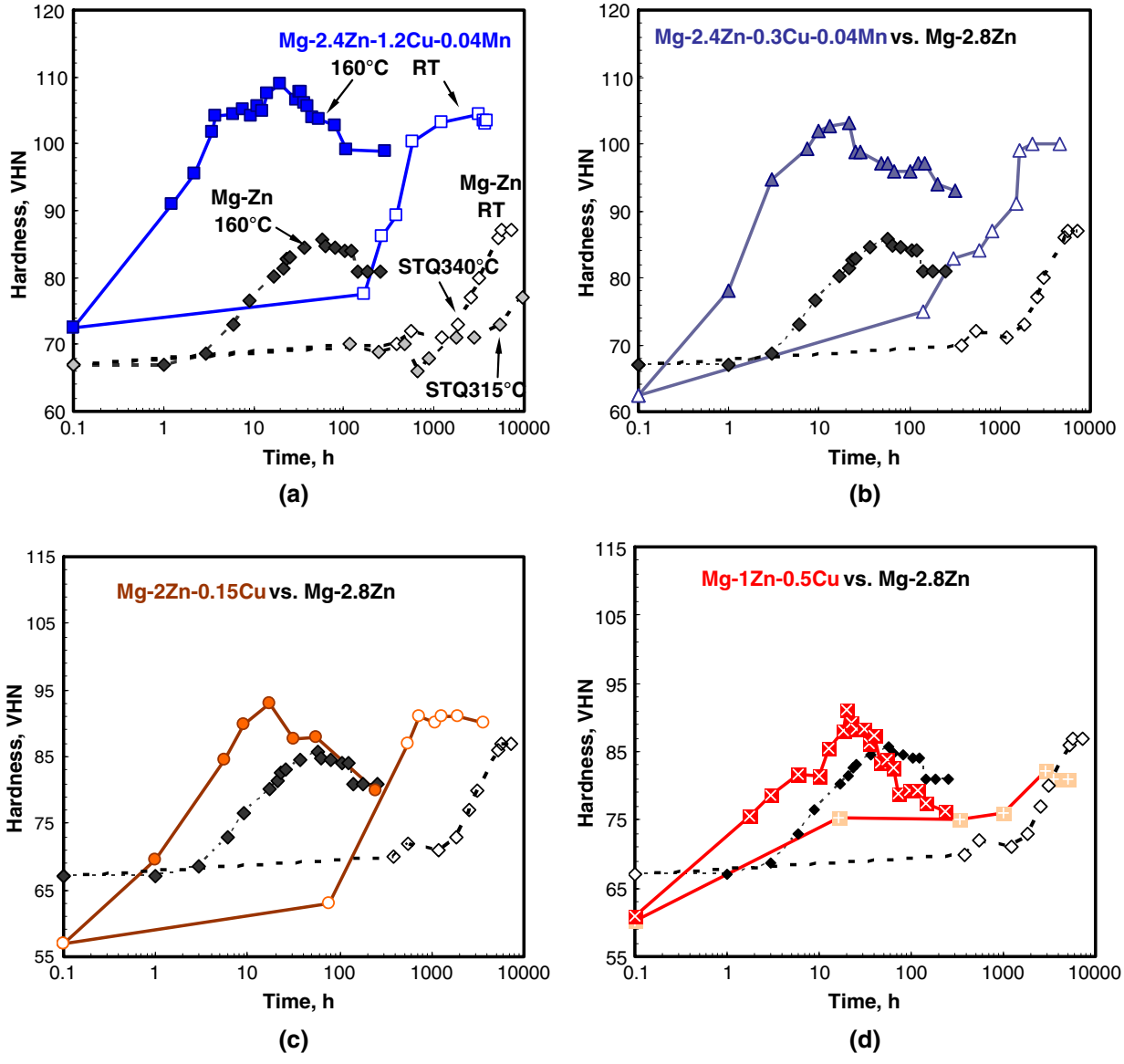

Fig. 1—Comparison of T6 (solid symbols) and T4 (open symbols) hardness curves between binary Mg-Zn alloy (diamonds) and Mg-Zn-Cu alloys: (*a*) alloy A (squares), (*b*) alloy B (triangles), (*c*) alloy C (circles), and (*d*) alloy D (crossed squares).

Table III. Analysis of Age-Hardening Responses (Hardness and Hardness Increments, VHN)

Alloy	STQ	Peak at 160 °C/Time, h	Increase from STQ	Increase from Mg-2.8Zn Peak	Maximum at RT/Time, Weeks	Increase at RT from STQ
Mg-2.8Zn	67	87/70	+20	—	77/56; 87/30	+10; +20
A: Mg-2.4Zn-1.2Cu-0.04Mn	72	109/20	+37	+22	104/7	+32
B: Mg-2.4Zn-0.3Cu-0.04Mn	62	103/20	+41	+16	100/5	+38
C: Mg-2Zn-0.15Cu	57	93/17	+36	+6	91/4	+34
D: Mg-1Zn-0.5Cu	60	91/20	+31	+4	82/16	+22

STQ—as-solution-treated and quenched condition.

III. RESULTS

A. *Age-Hardening Response*

The T6 and T4 hardness curves from binary Mg-Zn alloy and from Mg-Zn-Cu alloys are compared in Figure 1. The analysis of these measurements is presented in Table III. For the binary alloy, the peak hardness of 87 VHN was measured after about 70 hours of aging for both solution treatment temperatures (315 °C and 340 °C), and the hardness increment of 20 VHN was achieved relative to the as-solution-treated and quenched condition (Table III). Hardness curves (T6 and T4) for the alloy specimens quenched form 340 °C are plotted in Figure 1. As reported recently, hardness in the naturally aged condition of the binary alloy quenched from 340 °C equals that in the T6 condition after nearly 8 months of aging (open diamonds in Figure 1(a)).[16] Alloy quenched from 315 °C also undergoes natural aging (gray diamonds in Figure 1(a)); however, the kinetics of aging is considerably slower than for the specimen quenched from 340 °C, clearly due to a lower solutionizing temperature, therefore a lower supersaturation of vacancies in the as-quenched condition. All Cu-containing alloys exhibited considerably improved response to artificial aging and also underwent accelerated natural aging. These alloys were solutionized at temperatures that were 5 °C to 10 °C below their respective solidus temperatures. These temperatures were higher for alloys containing higher content of Cu (Table II). In the Cu-containing alloy A (Table I), the peak hardness of 109 VHN was measured after 18 hours of aging. After only 3 weeks of natural aging in this alloy, hardness exceeded 100 VHN (Figure 1(a)), and after 7 weeks, hardness reached 104 VHN. The hardness then remained at a similar level for the duration of the experiment (more than 2 years). Hardness plots shown in Figures 1(b) and (c) indicate that when the Cu content is reduced to almost a trace level, the alloys still harden rapidly at ambient temperature and the aging response at 160 °C is still enhanced compared to that of the binary alloy. Peak hardness of 103 VHN was measured after about 20 hours for alloy B (Figure 1(b)), which is double the hardness increment of the binary alloy relative to the as-quenched condition (Table III). Within 5 weeks of natural aging in the same alloy, the hardness reached 100 VNH and remained unchanged for the duration of the experiment (nearly 2 years). For alloy C containing a trace amount of Cu and no Mn (Figure 1(c)), after natural aging for 4 weeks, hardness (91 VHN) almost equaled that achieved during artificial aging (93) and remained unchanged for the duration of the experiment (more than 1 year). The result for alloy C also indicates that the remarkable natural aging in the Cu-containing alloys is not dependant on the presence of Mn, but primarily on the presence of Cu. Hardness plots from alloy D show that even when the Zn content (and the total solute content) is considerably reduced, the presence of Cu enhances the age-hardening response during artificial aging and accelerates the natural aging compared to the binary alloy (Figure 1(d)).

B. *Constituent Particles and Grain Size*

Figure 2 shows optical microscopy images of the as-solution-treated microstructures of the binary alloy and three Cu-containing alloys. The estimated ASTM grain size and the average number of grains per square millimeter in the solution-treated and quenched condition are given in Table IV. Coarse particles along the grain boundaries and within the grains in the binary alloy solution treated at 340 °C (Figure 2(a)) were consistent with the eutectic $Mg_{51}Zn_{20}$ (or Mg_7Zn_3) phase commonly observed in Mg-Zn alloys above the eutectoid temperature.[23] The particles in alloy A were finer and rounded and the grain size was considerably reduced compared to the binary alloy (Figure 2(b), Table IV). Similar particles were observed earlier in Mg-Zn-Cu alloys and referred to as the $Mg(Zn,Cu)_2$ eutectic phase that contributes to the grain refinement and improves the ductility in the as-cast condition.[3,4] This phase partially dissolves during solution heat treatment.[4] The TEM EDS analysis of a number of coarser particles showed that they contained 47 to 51 at. pct Mg, 31 to 33 at. pct Zn, 19 to 20 at. pct Cu, and about 0.1 at. pct Mn (Mn is added to Mg-Zn-Cu alloys to improve the tensile properties and corrosion resistance[3]). The fraction of these particles was reduced and the grain size slightly increased (Figure 2(c), Table IV) with the reduced amount of Cu in alloy B. Further reduction in the Zn and Cu contents, coupled with the absence of Mn in alloy C, resulted in an even greater reduction in the fraction of the constituent particles and increase in the grain size. The grain size of alloy D (not reported here) was considerably coarser than in the other alloys. These observations indicate that the fraction of the grain boundary Mg-Zn-Cu-Mn particles and the level of grain refinement are generally higher

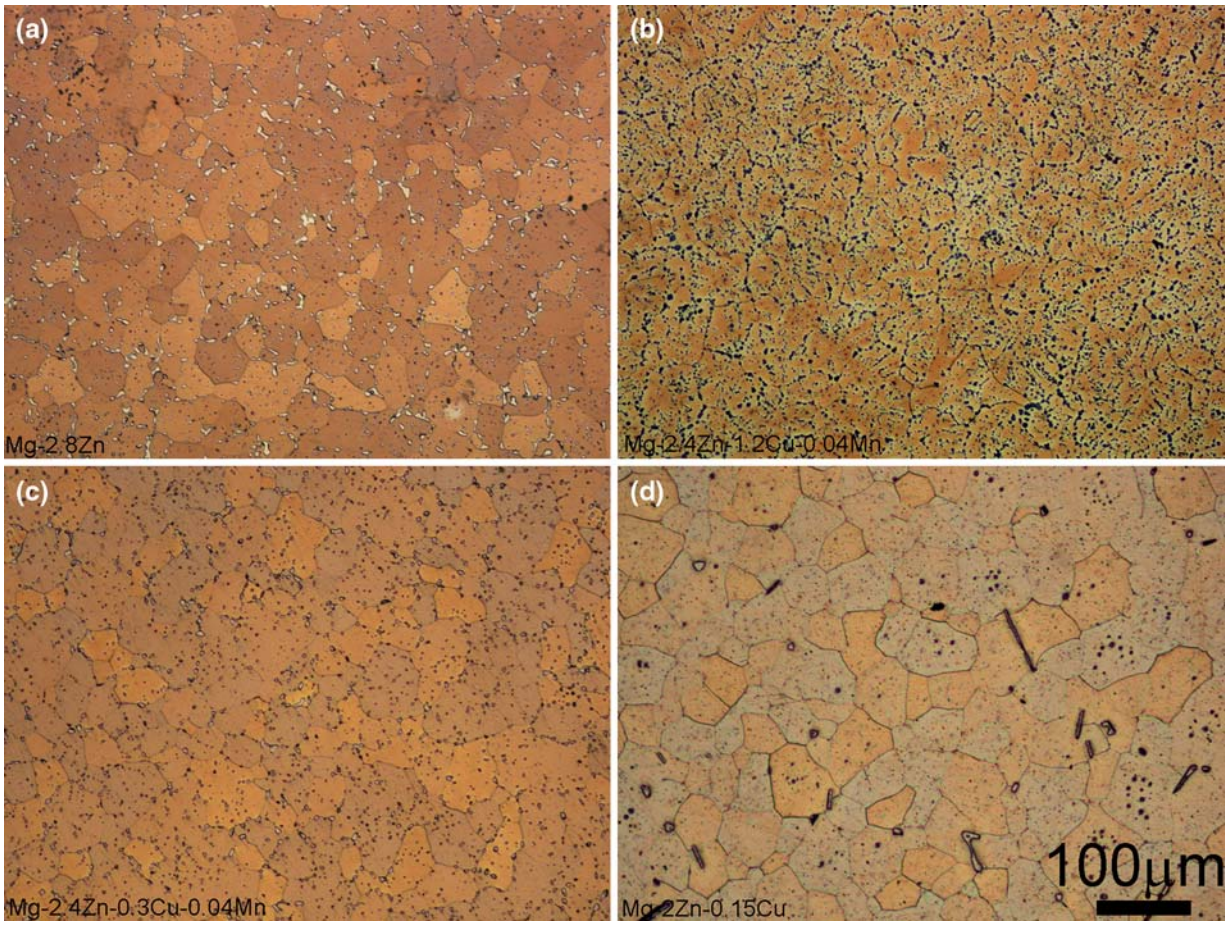

Fig. 2—Optical microscopy images of the solution-treated microstructures of alloys: (*a*) binary, (*b*) A, (*c*) B, and (*d*) C. All images were taken at the same magnification.

Table IV. ASTM Grain Size (*G*) and the Average Number of Grains per Square Millimeter ($\overline{N_A}$) for the Binary Alloy and Alloys A, B, and C in the As-Solution-Treated Condition

Alloy	Binary	A	B	C
G	6.4	6.7	5.9	4.7
$\overline{N_A}$	658	824	459	205

in the presence of higher Cu content for a similar Zn content. Due to the formation of these particles, the contents of Zn and Cu available for the precipitation within the grains are reduced accordingly.

C. *Microstructure Development during Artificial Aging*

1. *TEM observations*

The microstructures of all alloys aged to their T6 peak-hardness conditions are shown in Figure 3. The TEM images taken from a $[2\bar{1}\bar{1}0]_{Mg}$ direction (a, c, e, g, and i) show elongated precipitates perpendicular to a $(0001)_{Mg}$ plane, in earlier works, referred to as β'_1 rods and β'_2 laths, which were primarily responsible for the hardening in these alloys.[4,6–8,11,15,24,25] The images taken from a $[0001]_{Mg}$ direction (b, d, f, h, and j) show the same precipitates end-on. The cross section of the precipitates in all alloys studied was generally rectangular with a varying ratio of the rectangle sides, so that the precipitates appeared as rods (β'_1) and some also as laths (β'_1). Occasional coarse β'_2 precipitates parallel to a $(0001)_{Mg}$ plane were observed (the upper right corner in Figure 3(a); a plate arrowed in Figure 3(b); a six-sided plate arrowed in Figure 3(f)) along with a number of smaller blocky precipitates of most likely the β'_1 phase[11] perpendicular to a $(0001)_{Mg}$ plane (arrowed in Figures 3(a), (c), (d), (e), and (f)). The elongated precipitates in the binary alloy (Figures 3(a) and (b)) were very coarse (the median length was about 325 nm), very inhomogeneously distributed, and widely spaced. The density of the precipitates in this alloy also varied from one grain to another. On the other hand, the precipitates in the Cu-containing alloys were homogeneously distributed, far more densely dispersed, and as a result finer (the median length was about 48 nm for alloy A, 157 nm for alloy B, and 70 nm for alloy C) and more closely spaced. These observations are consistent with the previous work on similar alloys.[4,24] Figure 3(f) shows that in some areas of the specimen, the elongated precipitates were sequentially ordered and an increased density of these precipitates was occasionally observed along $\langle 0\bar{1}10\rangle_{Mg}$ directions. Similar arrays of the precipitates were occasionally observed in all alloys studied.

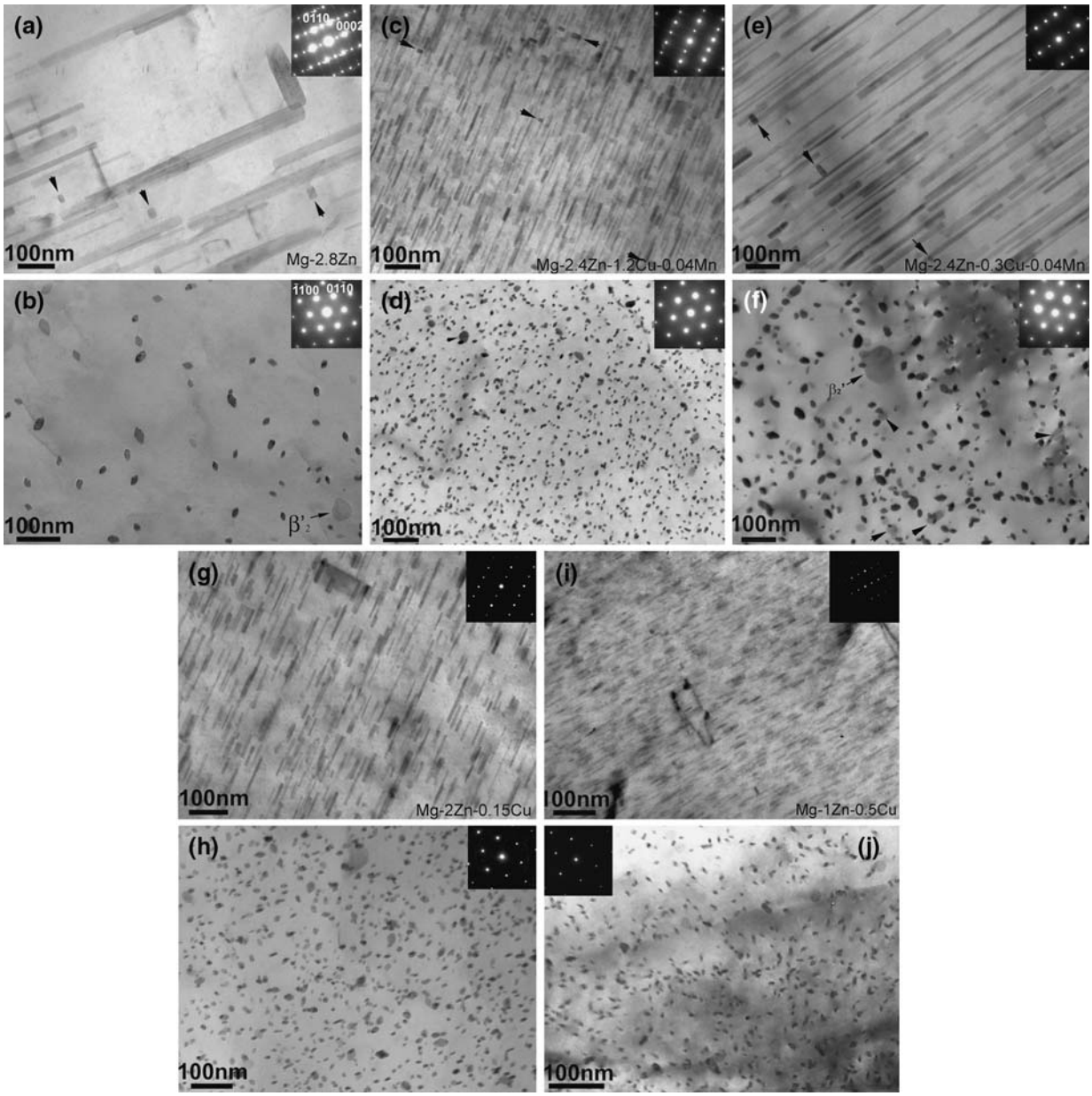

Fig. 3—TEM images showing the peak-aged T6 microstructures of (*a*) and (*b*) binary Mg-Zn alloy; (*c*) and (*d*) alloy A; (*e*) and (*f*) alloy B; (*g*) and (*h*) alloy C; and (*i*) and (*j*) alloy D. e^- beam $\| [2\bar{1}\bar{1}0]_{Mg}$ for (a), (c), (e), (g), and (i); and e^- beam $\| [0001]_{Mg}$ for (b), (d), (f), (h), and (j). Inset images are corresponding SAED patterns.

Clark[6] also observed arrays of the β'_1 rods from a direction almost perpendicular to a $\langle 0001 \rangle_{Mg}$ and ascribed this to nucleation on dislocations lines. Although nucleation on dislocations might be accounted for some of the arrays observed here, a repetitive arraying along directions that precisely align with the $\langle 0\bar{1}10 \rangle_{Mg}$ is unlikely to be associated with dislocations. Also, the arrayed precipitates do not appear to be coarser than the precipitates elsewhere in the grain, which would be the case if they were nucleated on dislocations due to higher diffusion rates. When volume fraction of precipitates is high, interactions between their strain fields may affect the precipitate growth, and as a result, the precipitates may be arrayed along certain directions or congregated on certain plains.[26] This may be the reason for the arraying of the precipitates reported here, which might have been induced by the interaction of the strain fields associated with the β'_1 nuclei, which then grew mainly by rod lengthening.[6]

From the images in Figure 3, it appears that there is a direct correlation between the number density and size of the precipitates and the alloy composition. The density of the β'_1 precipitates generally depended on the Cu content (higher for a higher Cu content). This indicates that Cu enhances the nucleation of the precipitates during artificial aging. The size, or the aspect ratio of these precipitates (the ratio of length to thickness), was, on the other hand, dependant on the Zn content and most likely the diffusivity of Zn to the Cu-Zn–induced nuclei (*e.g.*, for alloy D, the number density of the precipitates

was very high, but their length was much smaller than for the example in alloy B). Note that in alloy B, the fraction of the Cu-containing intermetallics was significantly greater than in alloy C (Figure 2); therefore, the actual Cu content within grains was significantly reduced (possibly even below that in alloy C), which explains a slightly lower apparent number density of the precipitates in this alloy compared to alloy C.

2. *3DAP observations*

The peak-aged microstructure of alloy A was further investigated by 3DAP. A field ion image (Figure 4(a)), obtained under a combination of Ne and H_2 imaging gases in the vicinity of the $(0\bar{1}10)_{Mg}$ pole, clearly reveals at lest two elongated (β'_1) precipitates visible as brighter contrast of the Zn (and Cu) atoms relative to the Mg atoms. Elemental maps showing the distributions of the Zn and Cu atoms are shown in Figure 4(b), and three Zn-rich precipitates were intercepted by the volume probed. The Cu enrichment within the precipitates was not as apparent from the atom map. It should be noted that, although a relatively small volume of alloy is probed by the 3DAP, the contents of Zn and especially that of Cu within the grains were found to be lower than the alloy bulk composition given in Table I. This is due to considerable amounts of Cu and Zn being incorporated into the constituent particles. The composition determined from the mass spectra of a number of data sets from the different artificially and naturally aged conditions was in the range 1.8 to 2.1 pct Zn, 0.08 to 0.22 pct Cu, and 19 to 55 ppm Mn (in at. pct), which depended primarily on whether some of the coarse precipitates (that incorporate the greatest amounts of Zn and Cu) were contained within the volume probed. The composition of one of the precipitates believed to be a β'_1 rod was determined by selecting a smaller volume of the data containing a section through the precipitate and the matrix either side of it, as indicated by a smaller colored box in the Zn map. From the ladder diagram (Figure 4(c)), the Zn content was found to be 49.3 pct, which is close to the stoichiometry of the MgZn phase, rather than that of the Mg_4Zn_7 or $MgZn_2$ phase reported for the β'_1 rods in the binary Mg-Zn alloys.[5,6,11] This result was confirmed in the peak-aged alloy D and alloy Mg-2Zn-2Cu-0.6Mn (in at. pct; not included in this publication). The Cu enrichment in the precipitate relative to the surrounding matrix of about 1.5 at. pct is also clear from the ladder diagram, while the Mn content was too low to be plotted (a few atoms only). An atom probe data from the coarse β'_1 rods in the binary alloy is needed in order to ascertain whether the phase stoichiometry may have been changed due to the presence of Cu atoms. It is possible that the composition of the precipitates in the binary alloy is also different from that reported in earlier studies. For example, in Al-Mg-Zn alloys, it was accepted for a long time that the composition of an intermediate η' phase was $MgZn_2$, *i.e.*, identical to that of the equilibrium η phase, and a number of crystal structures were determined by assuming a ratio 1Mg:2Zn. However, the 3DAP study by Stiller *et al.*[27] showed that the actual ratio in η' was close to 1Mg:1Zn. It is possible also that the composition of the

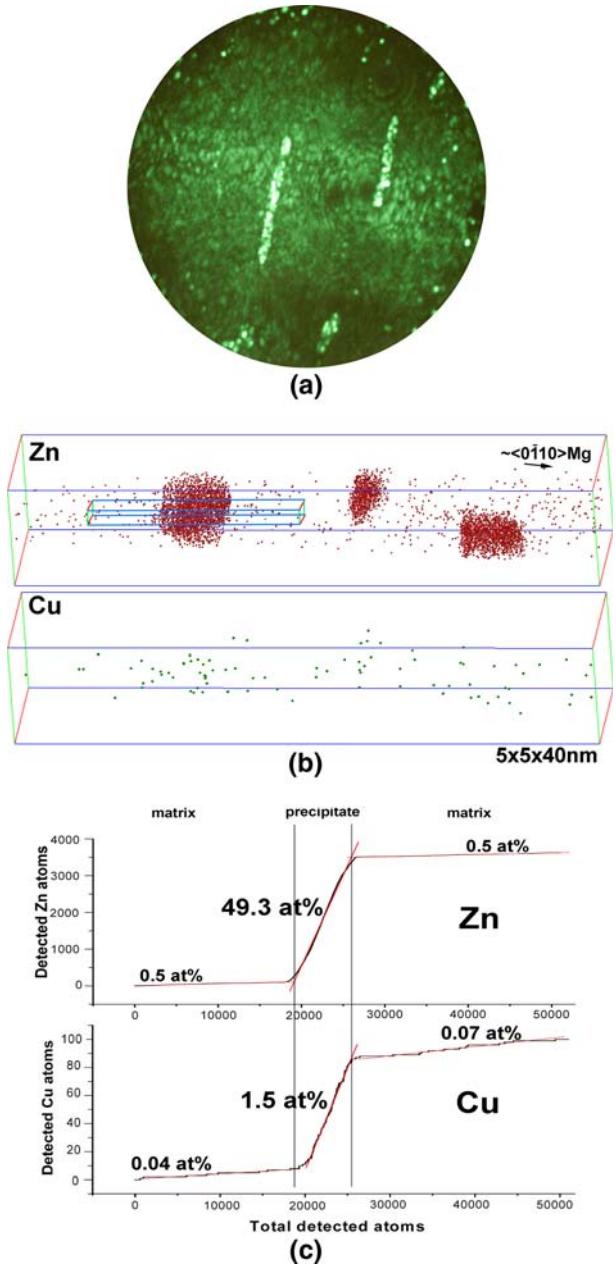

Fig. 4—(*a*) Ne and H_2 FIM image taken at 5.3 kV and 60 K from the specimen of alloy A aged to T6 peak hardness; (*b*) 3DAP elemental maps showing the distribution of Zn and Cu atoms; and (*c*) a ladder diagram constructed from one of the truncated β'_1 precipitates (selected in the Zn elemental map).

precipitates in Mg-Zn–based alloys changes with the alloy composition and heat treatment, as observed commonly in some aluminum alloys.[28,29]

D. *Natural Aging in Mg-Zn Alloy*

In the naturally aged binary alloy, very fine, up to 10-nm long, planar precipitates with an apparent thickness corresponding to one magnesium atomic layer were first occasionally observed by HRTEM on $\{2\bar{1}\bar{1}0\}_{Mg}$ planes with a $[0001]_{Mg}$ beam direction after about 5 weeks of aging. The HRTEM image in

Figure 5(a) shows these precipitates in the specimen naturally aged for 9 weeks. These precipitates were inhomogeneously distributed and present in a very low number density. These precipitates correlate well with the X-ray diffraction results by Takahashi *et al.*;[13] therefore, they will be referred to as GP1 zones. In the same specimen, precipitation in some grains was also observed by conventional TEM. Coarse, widely spaced, and inhomogeneously distributed precipitates are visible in Figure 5(b) taken from a $[0001]_{Mg}$ direction. Some of these precipitates were associated with dislocations (arrowed). Occasional sequential arraying of these precipitates along $\langle 0\bar{1}10\rangle_{Mg}$ directions, similar to that in the peak-aged alloys, was also observed. These precipitates exhibited a shape of a nonuniform prism and a high degree of coherency with $\{0\bar{1}10\}_{Mg}$ and $\{0001\}_{Mg}$ planes, as shown in Figures 5(c) and (d), taken from the specimen naturally aged for 3 months. The formation of the planar GP1 zones and the prismatic precipitates, therefore, induced the hardening at ambient temperature. However, their very low number density and inhomogeneous distribution were responsible for this hardening effect to be very limited for aging times up to 3 months (Figure 1), *i.e.*, aging times comparable to those in which the Cu-containing alloys reach the near T6 hardness. On prolonged aging, the number density of the precipitates increased.[12] Due to their continuous growth, the spacing between these particles decreases so that the hardness equals that in the T6 condition after nearly 8 months of aging.[16]

E. *Natural Aging in Mg-Zn-Cu Alloys*

1. *TEM and HRTEM observations*

In alloy A, after only 4 days of natural aging, some mottled contrast was visible in the TEM images taken from a $[2\bar{1}\bar{1}0]_{Mg}$ (Figure 6(a)) and from a $[0001]_{Mg}$ (Figure 6(b)) direction. Attempted HRTEM observations did not reveal any discernable precipitates; however, after 2 weeks of aging, the dotted contrast corresponding to precipitates or strain field induced by fine precipitates was more clearly observed by the conventional TEM (Figures 6(c) and (d)). The microstructure corresponding to the maximum hardness of alloy A measured during natural aging (104 VHN) is shown in Figure 7, and two different precipitate morphologies were observed: prismatic and planar (disc-shaped). The prismatic precipitates of about 5 nm in size (as viewed from a $[0001]_{Mg}$ direction) were observed in rows along $\langle 0\bar{1}10\rangle_{Mg}$ directions (Figure 7(a)). A lower density of the homogeneously

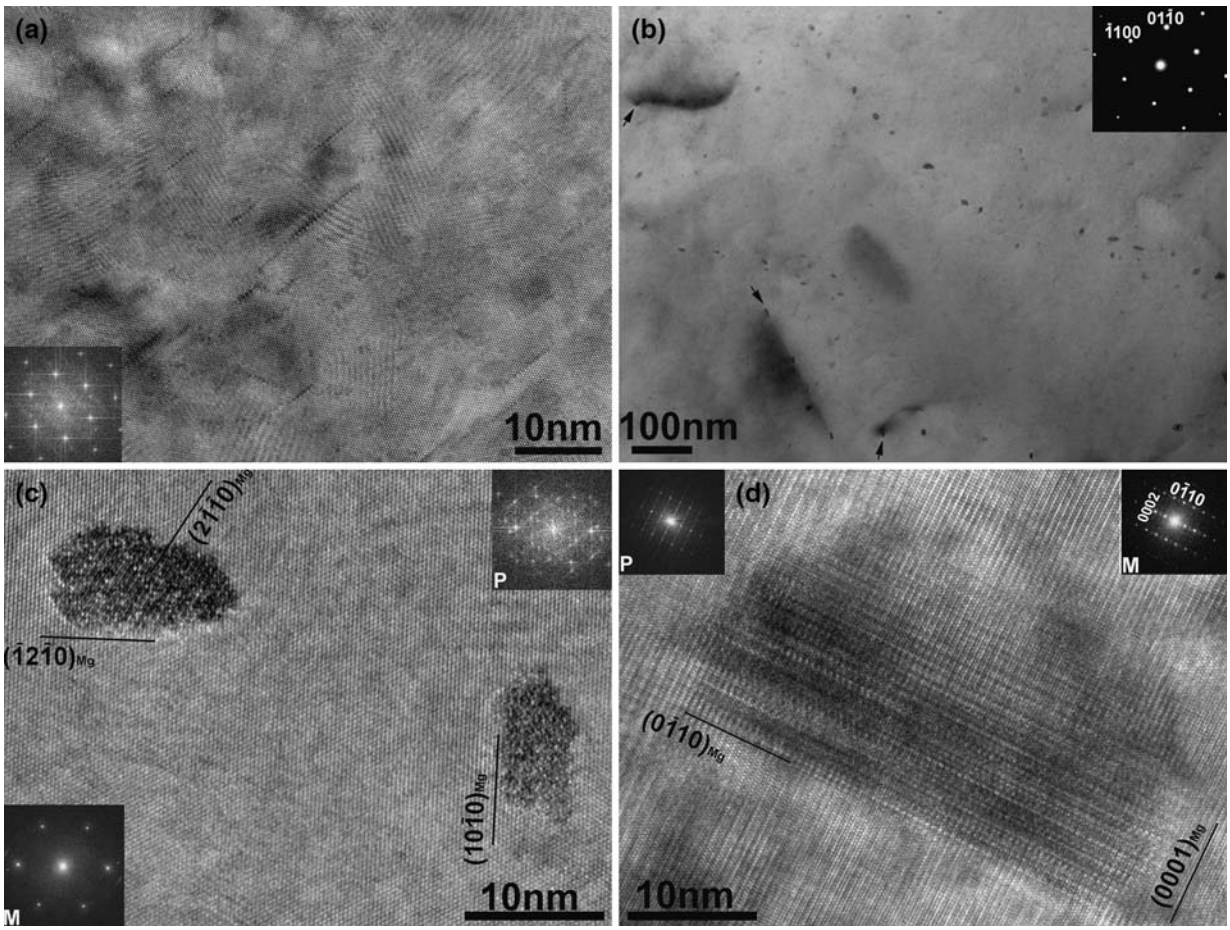

Fig. 5—$[0001]_{Mg}$ (*a*) HRTEM and (*b*) TEM images from the binary alloy naturally aged for 9 weeks; and (*c*) $[0001]_{Mg}$ and (*d*) $[2\bar{1}\bar{1}0]_{Mg}$ HRTEM images from the binary alloy naturally aged for 12 weeks. Insets in (a), (c), and (d) are the Fourier transforms (FFT) of the HRTEM images; M stands for the Mg matrix area and P for the precipitate area of the image. Inset in (b) is a recorded SAED pattern.

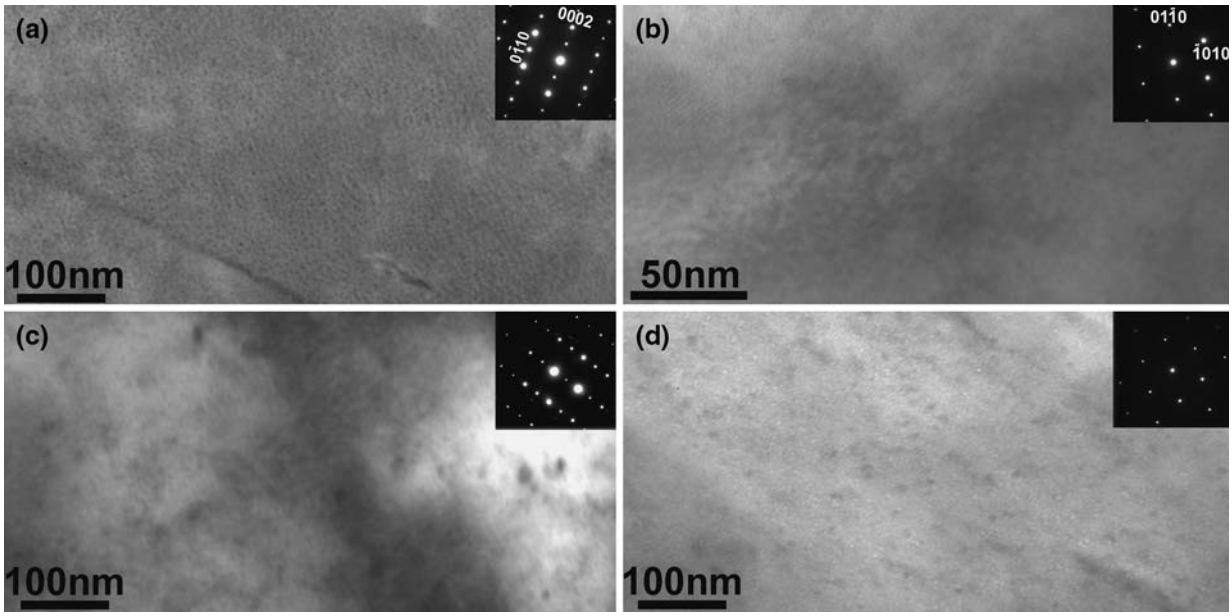

Fig. 6—TEM images from alloy A showing the evolution of the microstructure during the initial stages of natural aging: (*a*) and (*b*) after 4 days, and (*c*) and (*d*) after 2 weeks. e^- beam $\| [2\bar{1}\bar{1}0]_{Mg}$ for images on the left; and e^- beam $\| [0001]_{Mg}$ for images on the right. Inset images are corresponding SAED patterns.

distributed thin planar precipitates (up to approximately 30 nm in length/diameter) with a $(2\bar{1}\bar{1}0)_{Mg}$ habit plane was also observed (some coarser plates are arrowed in Figure 7(a)). These precipitates induced a considerable strain into the surrounding magnesium lattice, visible as a dark contrast along the sides of the precipitates. The TEM image taken from a $[\bar{1}2\bar{1}3]_{Mg}$ direction (Figure 7(c)) shows the planar precipitates viewed at 22.6 deg tilt from a $[0001]_{Mg}$ direction and reveals that their morphology is a disc (arrowed). A closer look at the area where the two rows of the prismatic precipitates intersect in Figure 7(a) revealed an extremely high density of finer planar precipitates (Figure 7(b)), homogeneously distributed on $\{2\bar{1}\bar{1}0\}_{Mg}$ planes. Figure 7(b) also indicates that the mottled contrast observed in the TEM images was induced by the overlapping strain fields associated with the fine planar precipitates (not clearly visible at lower magnifications by TEM). The HRTEM image taken from a $[0001]_{Mg}$ direction (Figure 7(d)) shows the fine planar precipitates (3 to 10 nm in diameter) and two of the coarser discs. These planar precipitates (both small and coarse ones) correspond well to GP1 zones. A smaller number of very fine presumably prismatic precipitates were also occasionally observed by HRTEM, and two of those are shown in the inset image in Figure 7(d).

The HRTEM images in Figure 8 taken with a $[2\bar{1}\bar{1}0]_{Mg}$ beam direction show planar precipitates parallel to a $(0001)_{Mg}$ plane, earlier referred to as GP zones,[14] in the naturally aged binary alloy (Figure 8(a)). Similar precipitates were occasionally observed also in alloy A. The density of these precipitates, however, was extremely low in both alloys, and they were only occasionally observed in some specimens; thus, their contribution to hardening was almost negligible compared to that of the GP1 zones and prismatic precipitates.

2. *3DAP observations*

The 3DAP data from alloy A naturally aged for 11 weeks are compared to those of the binary alloy naturally aged for the same amount of time in Figure 9. Figure 9(a) shows Zn and Cu elemental maps and a map where the regions with an increased solute density (precipitates) were selected and presented without the solute in the solid solution. A very high density of the regions enriched in both Zn and Cu is visible in the elemental maps. Some of these regions appeared as discs viewed at a high angle (outlined on some of the precipitates) and were placed at approximately 120 deg with respect to each other, which correlates well with the fine disclike GP1 zones observed by TEM in the specimen aged for 8 weeks. It should be noted that there was no significant difference in the hardness value between 8 and 11 weeks of aging (Figure 1(a)); thus, no significant difference between the corresponding microstructures is expected. A smaller fraction of the finer precipitates exhibiting the size (2 to 4 nm) and morphology, which can be correlated with the fine prismatic precipitates, and some fine (up to 2 nm) and diffuse Zn-Cu co-clusters containing not less than 20 solute atoms were also observed. The least numerous (~8 pct) were very diffuse Zn clusters containing up to about 20 atoms. The composition of some of the precipitates is indicated in Figure 9(a), numbered 1 through 4. Note that some precipitates were truncated, which reduces the reliability of the analysis result. It should also be noted that due to a significant difference in the evaporation fields of Zn and Cu relative to Mg,[30] the apparent content of Mg in the fine-sized precipitates is expected to be overestimated. Nevertheless, the common feature of all precipitates was that the ratio of Zn to Cu was very high, and it was found to increase with the increase in the precipitate size from

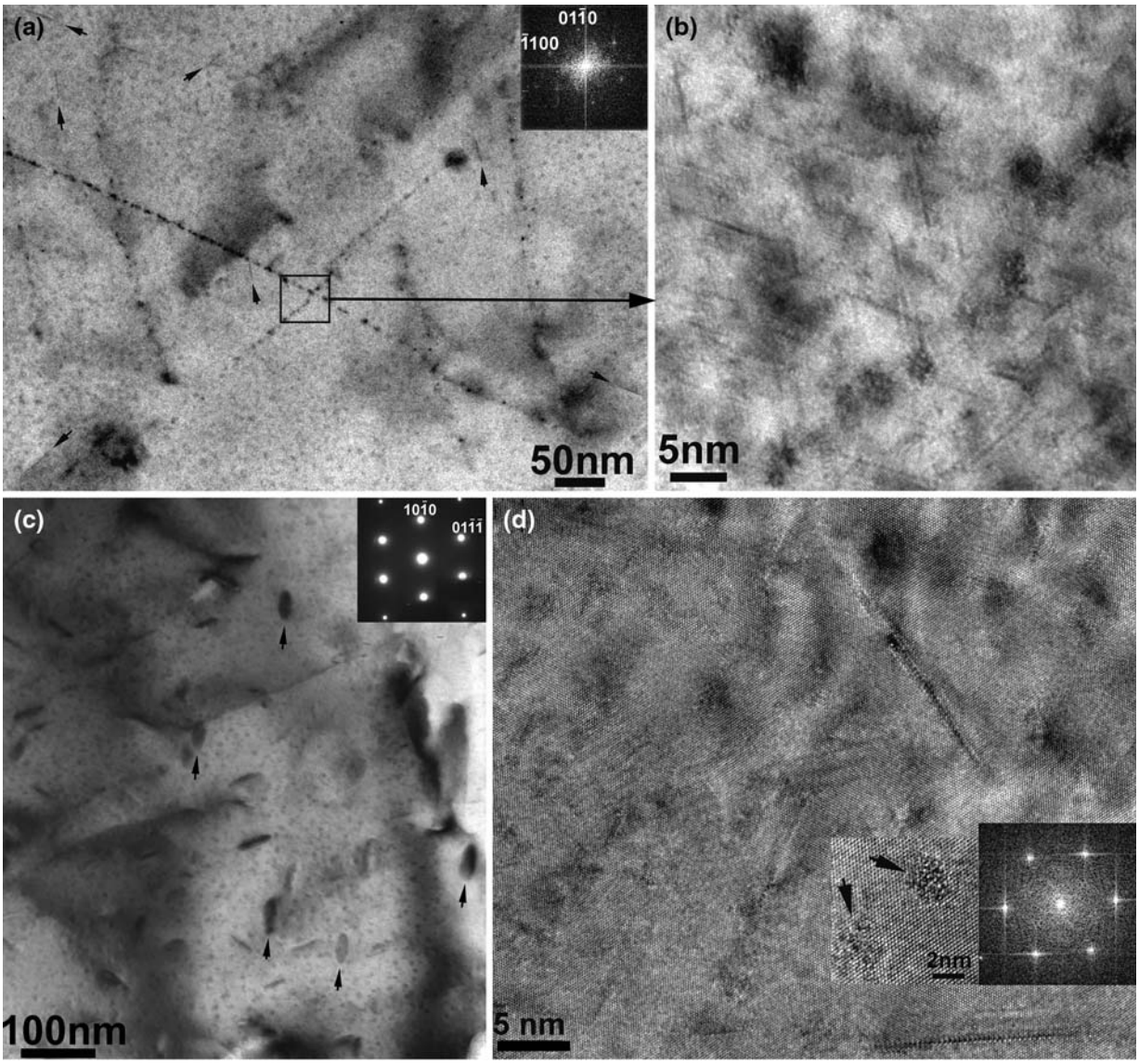

Fig. 7—(*a*) $[0001]_{Mg}$ TEM image; (*b*) and (*d*) $[0001]_{Mg}$ HRTEM images, and (*c*) $[\bar{1}2\bar{1}3]_{Mg}$ TEM image from alloy A naturally aged for 8 weeks (~104 VHN).

approximately 7:1 to 30:1 across all precipitate species. This suggests that the growth of the precipitates was controlled mostly by Zn diffusion, while Cu may have controlled their nucleation. Due to their composition (a considerably higher Zn than Cu content) and morphology, the planar/disc-shaped precipitates in the Cu-containing alloys are also referred to as the GP1 zones in this work. Some association of Mn with the precipitates was with certainty determined only in the two truncated coarse (~4 × 12 × ? nm) precipitates distinct in the lower right end of the atom maps. The compositional analysis of one of these precipitates, denoted 4 in the image, showed that it contained 27 pct Zn, 1.5 pct Cu, and 0.02 pct Mn (in at. pct). The number density of the precipitates for a number of probed specimens was in the range 3.5 to 5.7 × 10^{24} precipitates/m^3.

In the binary alloy naturally aged for 11 weeks (Figure 9(b)), apart from some diffuse Zn clusters containing about 30 Zn atoms, and one truncated coarser precipitate, the rest of Zn appeared to be dispersed in the solid solution and no extensive precipitation comparable to that in the Mg-Zn-Cu alloy had taken place in the volume analyzed. The Zn content determined from the mass spectrum was 2.394 at. pct, which is slightly lower than the alloy bulk composition due to the formation of the eutectic phase shown in Figure 2(a). On prolonged aging, a higher number density of the precipitates was observed in this alloy.[12] However, the precipitates remained inhomogeneously distributed throughout natural aging, and in some regions, a much higher number density of precipitates was observed than in others. For example, in a different volume of the same binary alloy aged for 16 weeks, a number of prismatic precipitates were observed along with some Zn clusters and the number density of the precipitates was of the order of 10^{23} precipitates/m^3.[12] However, due to the pronounced inhomogeneity in the precipitate distribution (based on low-magnification

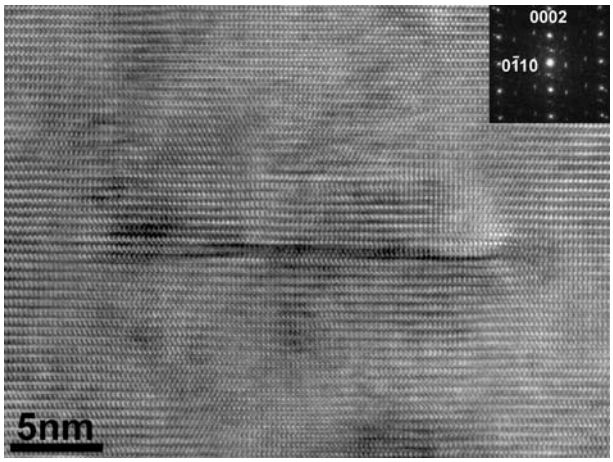

Fig. 8—$[2\bar{1}\bar{1}0]_{Mg}$ HRTEM image from the binary alloy naturally aged for 9 weeks.

observations by TEM), this value is unlikely to be representative of the bulk alloy.

The TEM and HRTEM images (Figure 10) taken from a $[0001]_{Mg}$ direction from alloy B naturally aged for 12 weeks (~100 VHN), in comparison to alloy A, indicate that the reduction in the Cu content resulted in an increased fraction of the prismatic precipitates, which were also considerably coarser than in alloy A, at the expense of the disclike GP1 zones, which were absent in their coarser form (>~10 nm in diameter).

IV. DISCUSSION

A. *Effect of Cu on the Precipitate Nucleation and Kinetics of Precipitation*

The addition of Cu to a Mg-Zn alloy significantly improves the mechanical properties in the T6 condition,[3,4] mainly by increasing the density of the strengthening precipitates, but also by reducing the grain size and modifying the grain boundary precipitates, which

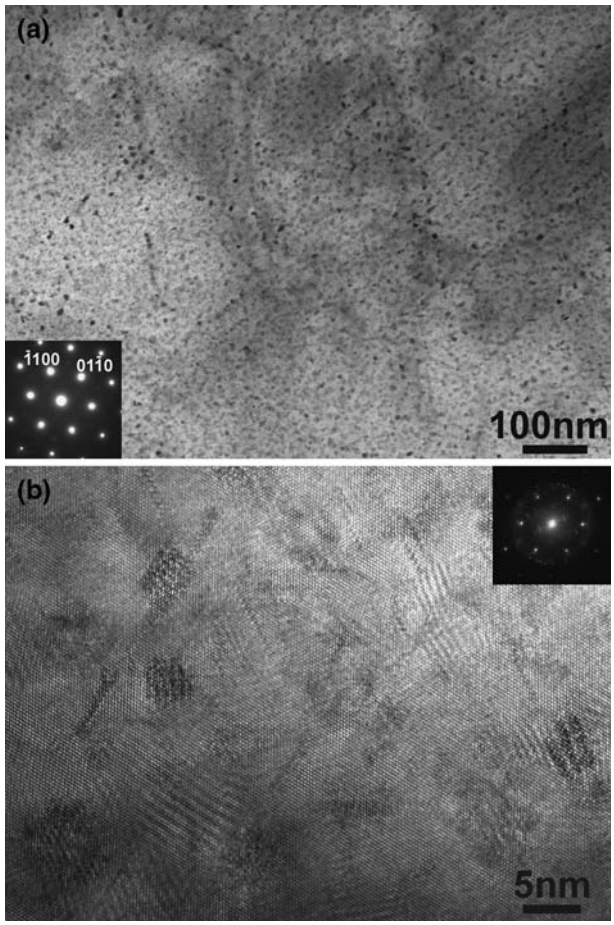

Fig. 10—$[0001]_{Mg}$ (*a*) TEM and (*b*) HRTEM images from alloy B naturally aged for 12 weeks (~100 VHN).

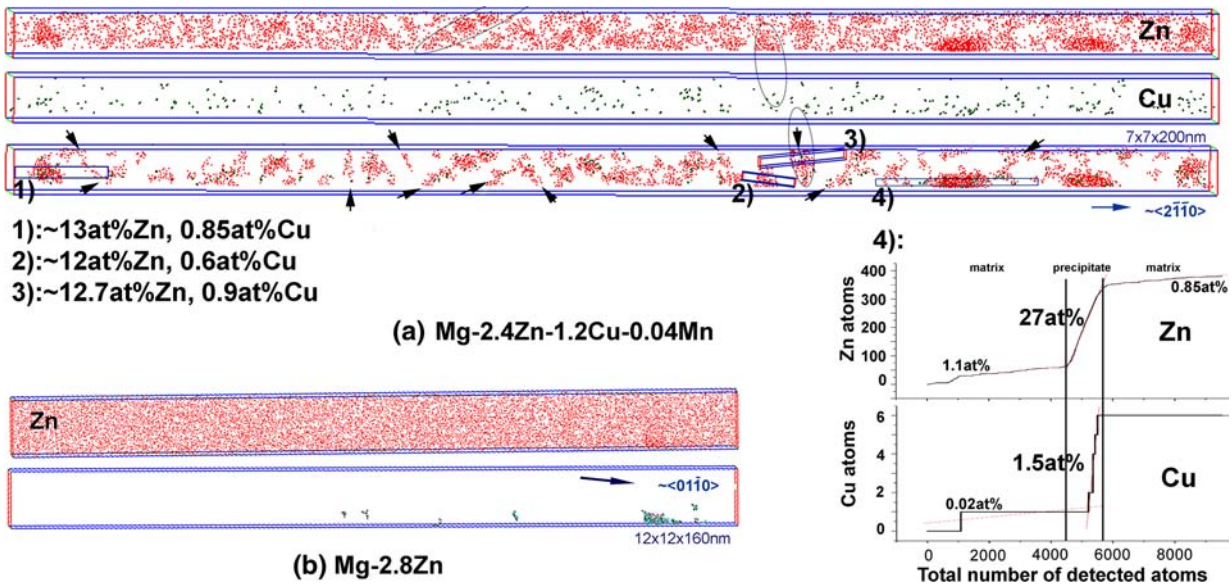

Fig. 9—3DAP elemental maps from (*a*) alloy A and (*b*) binary Mg-Zn alloy, both naturally aged for 11 weeks.

reduces grain boundary sliding. In the current work, the time to peak hardness was significantly reduced and the highest rate of hardening was achieved within the first hour of aging at 160 °C, as opposed to about 6 hours needed for the onset of hardening in the binary alloy. Compared to the binary alloy, the hardness increase from the solution-treated condition in the Cu-containing alloys with similar solute contents was almost doubled (Table III). The comparison between the microstructures of the artificially and naturally aged Mg-Zn and Mg-Zn-Cu alloys indicates that Cu enhances the nucleation of the precipitates and accelerates the kinetics of precipitation, in particular during natural aging. The nucleation of the precipitates and their dispersion, as well as the kinetics of precipitate nucleation and growth, are highly dependant on the distribution and concentration of vacancies.[26,31,32] Before considering the role of Cu in the nucleation process in more detail, it should be first noted that the addition of Cu to a Mg-Zn alloy increases the eutectic temperature, which permits the use of higher solution treatment temperatures[2] (Table II). This increases the vacancy supersaturation in the as-quenched condition of the Cu-containing alloys. Solute supersaturation is not likely to be significantly affected by the increase in the solution treatment temperature, because the maximal solubility of Zn in Mg of about 3.3 at. pct is at 340 °C[33] and the 3DAP data presented here show that the solute content in the Cu-containing alloys was close to, if not even lower than, the Zn content in the binary alloy. Therefore, one of the reasons for the rapid natural aging of the Cu-containing alloys is the increased supersaturation of vacancies in the as-quenched condition, *i.e.*, their higher solution heat treatment temperature compared to the binary alloy. Slower hardening of the binary alloy quenched from 315 °C than from 340 °C (Figure 1) is another clear indication of the effect of vacancy supersaturation on the magnitude and kinetics of natural aging.

Studies on aluminum alloys, however, show that unless there is a positive interaction between the solute and vacancies during or shortly after quenching, vacancies will migrate and disappear at the usual vacancy sinks (grain boundaries, matrix dislocations, dislocations associated with twin boundaries, sub-boundaries, matrix-intermetallic interfaces, *etc.*), and this would be expected to occur more readily when the diffusion distances are shortened (*e.g.*, the grain size reduced). Hardness measurements presented here also indicate that merely the difference in the solution treatment temperature is unlikely to be the sole reason for the accelerated natural aging and high hardness level of the Cu-containing alloys. For example, alloy B, which had a lower Cu and total solute content than alloy A, reached a hardness level almost equal to that of alloy A, and more importantly after a comparably short time, although it was quenched from a considerably lower temperature (Table II). Clark[6] observed that in the Mg-5 wt pct Zn alloy, quenching from 385 °C accelerated the nucleation of the β'_1 rods during subsequent artificial aging; however, these precipitates were still very coarse and inhomogeneously distributed, similarly to those in the specimen quenched from 315 °C. The magnitude of natural aging in Mg-Zn-Cu alloys therefore implies a positive interaction between the Cu or the Zn atoms and vacancies in the Mg matrix, which is enhanced by the presence of Cu, while the increased vacancy supersaturation only increases the probability of these interactions. Recently reported results from related studies also indicate that the alloy composition determines the kinetics (and magnitude) of natural aging to a far greater degree than the solutionizing temperature. For example, Ti-containing Mg-Zn alloy hardens rapidly at room temperature (within the 4- to 8-week time interval) even though it is quenched from the same temperature as the simple binary Mg-Zn alloys (*i.e.*, 340 °C).[16] On the other hand, Mg-Zn-Ba alloy shows very little difference from the binary alloy and it requires many months to reach near T6 hardness even when quenched from 440 °C.[34] Although the distribution of the precipitates in this alloy was homogeneous after about 4.5 months of aging, the kinetics of natural aging was not enhanced by the high supersaturation of vacancies in the as-quenched condition, which suggests that Ba in combination with Zn may not be very effective in retaining vacancies in the solid solution (as much as Cu or Ti are).

Lomer[31] proposed that in dilute alloys, the formation energy for a vacancy near the solute atom is lower than near the solvent atoms; thus, the vacancy concentration near the solute atoms is increased exponentially with the solute atom-vacancy binding energy. In turn, this increases a mean jump rate of vacancies near the solute atoms, known also as Johnson effect, so that the self-diffusivity of the solvent element in dilute alloys would also be enhanced.[35] This may suggest that, for an alloy containing more than one alloying element, the diffusivity of all elements may effectively be increased. However, studies on aluminum alloys show that the vacancy-solute interactions in this case are highly complex and depend on the type and quantities of the solute elements and that a strong vacancy binding energy of a solute element is not a guarantee for the enhanced diffusion processes. The addition of a trace amount of Mg to an Al-Cu alloy, for example, significantly enhances the natural aging response.[31] This was attributed to an increased diffusivity of Cu, necessary for the GP zone formation during natural aging, as a result of strong Mg-vacancy and Mg-Cu–vacancy interactions.[31] However, when trace amounts of Sn, Cd, or In, that have higher vacancy-binding energies in aluminum than Mg or Cu, are added to an Al-Cu alloy, natural aging is retarded,[36,37] because the majority of the vacancies were strongly bound to the trace elements and therefore unavailable for the diffusion of Cu.[38] The current study suggests that the diffusivity of Zn in the magnesium lattice is enhanced as a result of the Cu presence. This may be due to either a high affinity between the Cu atoms and vacancies in magnesium or strong Cu-Zn–vacancy interactions.

The density of the precipitates in Mg-Zn-Cu alloys generally depended on the Cu content, and as the analysis of the atom probe data showed, the Cu content in the precipitates increased with the precipitate size, but so did the Zn to Cu ratio. This suggests that the precipitate nuclei may have been formed by the

Cu-vacancy or the Cu-Zn–vacancy complexes, which then grew by the diffusion of primarily Zn and Mg (and Cu to a lesser extent). Due to a very low solubility of Cu in Mg, which is between about 0.12 and 0.21 at. pct in the pure solid magnesium at 440 °C,[33] it is likely that the Cu atoms dissociate from the magnesium matrix sooner and with a greater thermodynamic driving force than the Zn atoms and are, therefore, in a good position to immediately interact with vacancies during or shortly after quenching. The size of the Cu atom (~256-pm diameter) is also considerably smaller than that of the Mg atom (~320-pm diameter) and slightly smaller than that of the Zn atom (~268-pm diameter), so that the accommodation of a Cu cluster or a Cu-Zn co-cluster into the Mg lattice would necessitate the presence of vacancies to relieve the lattice strains. Such vacancy-solute complexes are more likely to become stable nuclei, because the presence of vacancies reduces the free energy for homogeneous nucleation by reducing the strain component, and also because these vacancies can be released back into the solid solution and repeatedly used to acquire more solute atoms. This mechanism of assisted nucleation is very similar to that involved with the heterogeneous nucleation on dislocations, also observed occasionally during natural aging in this work, where the presence of a dislocation minimizes the strain energy factor[39] and allows for the substantially increased diffusion of the solute along the dislocation line.[40]

It is likely that the densely distributed and vacancy-rich Cu-Zn nuclei would grow more readily and the kinetics of the precipitation would be noticeably accelerated. Experimental data obtained using positron annihilation spectroscopy techniques confirm strong interactions between the solute and vacancies in aluminum alloys, which continue far beyond the short period immediately after quenching.[41–43] According to these results, solute atoms and vacancies form pairs and co-clusters from which vacancies may be gradually released back into the matrix and reused for the diffusion processes over a longer period of time (weeks at reduced temperatures). It is plausible, therefore, that in Mg-Zn-Cu alloys, a considerable amount of vacancies that are most likely retained by the nuclei and the solute atoms are gradually reused over a period of several weeks to relieve the high solute supersaturation. In the binary alloy, however, although the level of solute supersaturation was comparable to that in the ternary alloys, the precipitation during natural aging required a considerably longer aging time. This indicates a reduced number of homogeneously and densely dispersed stable nuclei and a lack of vacancies to aid the growth of the nuclei, which points to a weaker interaction between Zn and vacancies in the absence of Cu.

B. *Precipitates and Strengthening in the T4 Condition*

Interaction between the gliding dislocations and the precipitates in magnesium alloys in the T6 condition involves mainly by-passing and the Orowan model for the precipitation strengthening by widely spaced strong noncoherent precipitates applies. Consequently, the strength levels achieved are considerably lower than in aluminum alloys in which the strengthening occurs *via* the combination of shearing and by-passing of a high dispersion of fine (semi-)coherent precipitates. An increase in the number density of the β'_1 precipitates (decrease in the interparticle spacing) in the Cu-containing alloys and the homogeneity of their dispersion can be accounted for by the increased hardening in the case of both by-passing and shearing.

In the T4 condition of the Mg-Zn-Cu alloys, however, the size (up to ~30 nm), the type (coherent discs and partially coherent prisms perpendicular to the main slip plane of Mg), and the spacing between the precipitates (of the order of the precipitate size) indicate that the reaction with the gliding dislocation would involve shearing and the model based on the theory of Mott and Nabarro would apply (coherency, chemical, stacking fault, modulus, and order strengthening).[26,44] Four types of precipitates that contribute strengthening were observed in the binary and ternary alloys: disc-shaped GP1 zones and the prismatic precipitates, both forming on the prismatic planes of the Mg lattice; very fine and fully coherent Zn-Cu co-clusters/Zn clusters; and occasionally very sparse planar GP zones on the basal planes. The HRTEM and atom probe observations indicate that the GP1 zones were most likely composed of the Zn (and Mg) layer(s), while the prismatic precipitates were a more complex phase composed of Zn and Mg atoms, with a smaller fraction of the Zn atoms in both types of the precipitates being replaced by the Cu atoms in the Mg-Zn-Cu alloys. The composition of the prismatic precipitates in alloy A was very similar to that of the prismatic precipitates in the binary alloy,[12] *i.e.*, very close compositionally to the stoichiometry of the eutectic Mg_7Zn_3 phase (containing also some Cu).

The disc morphology of the GP1 zones is not surprising considering the large atomic misfit ($\gg$5 pct) between Mg and both Zn and Cu, because a disc would be a minimum energy shape for a highly strained precipitate.[26] The separation between such precipitates is often of the order of disc diameter, which would be about 5 to 30 nm in the present case, and a considerable elastic stain would be induced into the Mg lattice, as seen in Figures 7 and 8. Based on the TEM and HRTEM observations, GP1 zones form prior to, but evolve simultaneously with, the prismatic precipitates. In alloy A (Cu-rich), GP1 zones were dominant over the prismatic precipitates and also more densely dispersed; thus, they made the major contribution to strengthening in this alloy. The comparison between alloys A (Cu rich) and B (similar to A but Cu lean) indicates that the higher Cu addition preferentially promotes the formation of GP1 zones, which then grow coarser and, thus, more closely spaced for the unchanged volume fraction, while the reduced Cu level results in the formation of an increased fraction of the prismatic precipitates. The prismatic precipitates in alloy B are also very densely and homogeneously distributed so the hardness level is comparable to that produced in alloy A mainly by a dense dispersion of a different type of precipitate. A significant strengthening by a fine dispersion of the GP zone type precipitates is not surprising. For example, in Al-Cu-Li-Ag-Mg-Zr alloys, the mechanical properties achieved after natural aging (for several

years) can reach that of the artificially aged material.[17] Likewise, in the Mg-Zn–based alloys, natural aging results in a very favorable combination of the tensile properties (an appreciably high yield strength and very high ductility even in cast alloy), and these results are presented elsewhere.[45]

V. CONCLUSIONS

1. The Mg-Zn-Cu alloys are among the Mg-Zn–based alloys that undergo accelerated hardening at ambient temperature (hardness in the T4 condition nearly equals that in the T6 after 4 to 8 weeks).
2. The addition of Cu to Mg-Zn alloy promotes the nucleation of an increased number density of the precipitates, as reported earlier. Due to most likely positive interactions of Cu and Zn atoms with vacancies, and thus increased retention of vacancies after quenching, the kinetics of precipitation is accelerated and the diffusivity of Zn enhanced in the presence of Cu.
3. The current results confirm that the kinetics of precipitation during natural aging depends primarily on the alloy composition (*i.e.*, on the additional alloying elements present in Mg-Zn alloy) and to a lesser degree on the solution heat treatment temperature (*i.e.*, the supersaturation of vacancies in the as-quenched condition).
4. Naturally aged Mg-Zn-Cu alloys are strengthened mainly by the formation of the coherent disc-shaped GP1 zones and generally prismatic semicoherent precipitates, both of which form on the prismatic planes of magnesium. GP1 zones are the predominant precipitates in alloy with a higher level of Cu. At a lower Cu content, the prismatic precipitates are represented more than the GP1 zones.
5. The 3DAP data indicate that the precipitates in the T4 condition of Mg-Zn-Cu alloy are formed from Cu-induced nuclei, which then grow through enrichment in primarily Zn and Mg (and Cu to a lesser degree).
6. The composition of the planar GP1 zones in the Mg-Zn-Cu alloy is close to 12 to 13 at. pct Zn and 0.6 to 0.9 at. pct Cu (the reminder being Mg, although the Mg content is likely to be overestimated), as determined by the 3DAP. The prismatic precipitates contained 27 at. pct Zn and 1.5 at. pct Cu, *i.e.*, their composition was close to the stoichiometry of the eutectic Mg_7Zn_3 phase (containing also some Cu).
7. The composition of the β'_1 rods in the artificially aged Mg-Zn-Cu alloy is close to that of the MgZn phase with about 1.5 at. pct Cu also being present (*i.e.*, it is different from that of the Mg_4Zn_7 or $MgZn_2$ phases, as reported in earlier works).

ACKNOWLEDGMENT

This work was funded by the Japan Society for the Promotion of Science (JSPS) in the form of a JSPS Postdoctoral Fellowship held by one of the authors (JB).

REFERENCES

1. N.K. Suseelan and M.C. Mittal: *Mater. Sci. Forum*, 1988, vol. 30, pp. 89–103.
2. W. Unsworth: *Light Met. Age*, 1986, vol. 8, pp. 10–13.
3. W. Unsworth and J.F. King: *Magnesium Technology*, Institute of Metals, London, 1987, pp. 25–31.
4. G.W. Lorimer: *Magnesium Technology*, Institute of Metals, London, 1986, pp. 47–53.
5. L. Sturkey and J.B. Clark: *J. Inst. Met.*, 1959–60, vol. 88, pp. 177–81.
6. J.B. Clark: *Acta Metall.*, 1965, vol. 13, pp. 1281–89.
7. G. Mima and Y. Tanaka: *Trans. JIM*, 1971, vol. 12, pp. 71–75.
8. G. Mima and Y. Tanaka: *Trans. JIM*, 1971, vol. 12, pp. 76–81.
9. J. Gallot: Ph.D. Thesis, University of Rouen, Rouen, France, 1966.
10. M. Bernole, J. Gallot, and R. Graf: *J. Microsc.*, 1965, vol. 4, pp. 787–92.
11. X. Gao and J.F. Nie: *Scripta Mater.*, 2007, vol. 56, pp. 645–48.
12. J. Buha: *Mater. Sci. Eng. A*, 2008, DOI 10.1016/j.msea.2008.02.038, in press.
13. T. Takahashi, Y. Kojima, and K. Takanishi: *Jap. J. Inst. Light Met.*, 1973, vol. 23, pp. 376–82.
14. I.J. Polmear: *Light Alloys: Metallurgy of the Light Metals*, 3rd ed., Arnold, London, 1995, p. 204.
15. E.O. Hall: *J. Inst. Met.*, 1968, vol. 96, pp. 21–27.
16. J. Buha: *J. Mater. Sci.*, 2008, vol. 43, pp. 1220–27.
17. K.S. Kumar and F.H. Heubaum: *Acta Mater.*, 1997, vol. 45 (6), pp. 2317–27.
18. *ASM Specialty Handbook, Magnesium and Magnesium Alloys*, ASM INTERNATIONAL, ASM, Materials Park, OH, 1998, p. 27.
19. http://ddsdx.uthscsa.edu/dig/itdesc.html.
20. O. Jagutzki, A. Cerezo, A. Czasch, R. Doerner, M. Hattass, M. Huang, V. Mergel, U. Spillmann, K. Ullmann-Pfleger, T. Weber, H. Schmidt-Boecking, and G.D.W. Smith: *IEEE Trans. Nucl. Sci.*, 2002, vol. 49, pp. 2477–83.
21. O. Jagutzki, H. Schmidt-Boecking, V. Mergel, A. Cerezo, and M. Huang: UK Patent 0003261.5, Aug. 15, 2001.
22. http://www.oxfordnanoscience.com.
23. L.Y. Wei, G.L. Dunlop, and H. Westengen: *Metall. Mater. Trans. A*, 1995, vol. 26A, pp. 1947–55.
24. R.I. Moss: Ph.D. Thesis, University of Manchester, Manchester, UK, 1983.
25. L.Y. Wei, G.L. Dunlop, and H. Westengen: *Metall. Mater. Trans. A*, 1995, vol. 26A, pp. 1705–16.
26. A. Kelly and R.B. Nicholson: *Progr. Mater. Sci.*, 1963, vol. 10 (3), pp. 151–391.
27. K. Stiller, P.J. Warren, V. Hansen, J. Agenete, and J. Gjønnes: *Mater. Sci. Eng. A*, 1999, vol. A270, pp. 55–63.
28. S. Esmaeili, D. Vaumousse, M.W. Zandbergen, W.J. Poole, A. Cereso, and D.J. Lloyd: *Phil. Mag.*, 2007, vol. 87, pp. 3797–3816.
29. J. Buha, R.N. Lumley, and A.G. Crosky: *Phil. Mag.*, 2008, vol. 88, pp. 373–90.
30. M.K. Miller, A. Cerezo, M.G. Hetherington, and G.D.W. Smith: *Atom Probe Field Ion Microscopy*, Clarendon Press, Oxford, United Kingdom, 1996, p. 492.
31. W.M. Lomer: *Inst. Met. Monograph Rep. Ser.*, 1958, vol. 23, pp. 79–97.
32. J.D. Embury and R.B. Nicholson: *Acta Metall.*, 1965, vol. 13, pp. 403–17.
33. M. Hansen, written in cooperation with K. Anderko: *Constitution of Binary Alloys*, 2nd ed., McGraw-Hill Book Co., New York, NY, 1958, p. 929.
34. J. Buha: Mater. *Sci. Eng. A*, 2008, DOI 10.1016/j.msea.2008.01.027, in press.
35. R.E. Hoffman, D. Turnbull, and E.W. Hart: *Acta Metall.*, 1955, vol. 3, pp. 417–24.
36. H.K. Hardy: *J. Inst. Met.*, 1951–52, vol. 80, pp. 483–87.
37. H.K. Hardy: *J. Inst. Met.*, 1955–56, vol. 84, pp. 429–33.

38. H. Kimura and R.R. Hasiguti: *Acta Metall.*, 1961, vol. 9, pp. 1076–79.
39. J.W. Chan: *Acta Metall.*, 1957, vol. 5, pp. 169–72.
40. F. Seitz and D. Turnbull: *Solid State Physics*, Academic Press, New York, NY, 1956, vol. 3, p. 226.
41. R. Ferragut, A. Somoza, A. Dupasquier, and I.J. Polmear: *Mater. Sci. Forum*, 2002, vols. 396–402, pp. 777–82.
42. C.E. Macchi, A. Somoza, A. Dupasquier, and I.J Polmear: *Acta Mater.*, 2003, vol. 51, pp. 5151–58.
43. J. Buha: Ph.D. Thesis, University of New South Wales, Sydney, Australia, 2005, available at http://adt.caul.edu.au, p. 177.
44. A.J. Ardell: *Metall. Trans. A*, 1985, vol. 16A, pp. 2131–65.
45. J. Buha: *Mater. Sci. Eng. A*, 2008, Doi: 10.1016/j.msea.2007.12.006, in press.